

This equation is used to determine the experimental values for the deformations appearing in  $Q_0$ . In Sec. 2.8.6 we saw that they agree with the theoretically determined deformations. Therefore, the particle-plus-rotor model gives the proper  $E2$  transition probabilities for transitions with the same  $K$ -value.

For transitions with different  $K$ -values, the collective part vanishes. Such transitions are, in fact, very weak ( $K$ -*forbidden*) because the single-particle part contains only the single-particle matrix element of  $r^2 Y_{20}$  in the intrinsic frame. We have already seen in Section 2.7.2 that they are small compared to the collective values. On the other hand, a pure single-particle model cannot explain the effective charges in spherical nuclei (see Sec. 2.7.2). The same difficulties occur here again. For a detailed discussion, see the paper of Löbner and Malinskog [LM 66], which contains much experimental data together with possible ways to improve the simple Nilsson estimate.

Finally, we have to mention that the above considerations apply only to pure  $K$ -bands. For transition probabilities and electromagnetic moments in  $K$ -mixed bands, like rotational aligned bands or bands in an asymmetric rotor, we have to take into account the mixing coefficients.

### 3.4 The Cranking Model\*

We have seen in the last section how the motion of particles in a deformed well can be connected with the idea of a rigid rotor. This model is very successful in the description of the level structure of rotational and even transitional nuclei. However there exists no straightforward microscopic derivation; in particular, one cannot calculate the inertial parameters in this model.

On the other hand, nearly all fully microscopic theories of nuclear rotation are based on or related in some way to the cranking model, which was introduced by Inglis [In 54, 56] in a semiclassical way, but as we shall see in Section 11.4, it can be derived fully quantum mechanically, at least in the limit of large deformations, and not too strong  $K$ -admixtures ( $K \ll I$ ).

The cranking model has the following advantages.

- (i) In principle, it provides a fully microscopic description of the rotating nucleus. There is no introduction of redundant variables, therefore, we are able to calculate the rotational inertial parameters microscopically within this model and get a deeper insight into the dynamics of rotational motion.
- (ii) It describes the collective angular momentum as a sum of single-particle angular momenta. Therefore, collective rotation as well as single-particle rotation, and all transitions in between such as decoupling processes, are handled on the same footing.
- (iii) It is correct for very large angular momenta, where classical arguments apply (even if the quantum mechanical derivation does not work in this limit [BMR 70]).

\* In this chapter, we treat only cranking theory for rotations. We can, however, also apply a similar theory for general collective motions, as discussed in Section 12.3.7.

The shortcomings of the model are:

- (i) As we shall see, it is basically a nonlinear theory. Only in the limit of small angular momenta can one linearize it using perturbation theory (cranking formula for the moment of inertia). In general, the calculations are therefore complicated, especially in cases where one has several solutions.
- (ii) The resulting wave functions are not eigenstates of the angular momentum operators. It is therefore not clear a priori how one has to calculate, for example, electromagnetic transition probabilities. In fact, we shall see in Section 11.4 that cranking model wave functions are in a sense only *internal wave functions* and that one has to use projection techniques to get the wave functions in the laboratory system.

In the following we shall give the usual semiclassical derivation (see, for instance, [Vi 57b, So 73]) and discuss the cranking model in connection with a pure single-particle Hamiltonian. Many of the arguments in the next sections can, however, also be applied to a general two-body Hamiltonian (see Sec. 7.7).

### 3.4.1 Semiclassical Derivation of the Cranking Model

The basic idea of the cranking model is the following classical assumption: If one introduces a coordinate system which rotates with constant angular velocity  $\omega$  around a fixed axis in space, the motion of the nucleons in the rotating frame is rather simple if the angular frequency is properly chosen; in particular, the nucleons can be thought of as independent particles moving in an average potential well which is rotating with the coordinate frame.

In Section 11.4, we will see how the consequences of this picture can also be derived from quantum mechanics using projection techniques. For the moment, however, we want to stay with the classical description because of its intuitive character. Also, we do not want to take into account any residual interaction. Therefore, we assume a single-particle potential  $V$  of fixed shape, which rotates in space, and accordingly we must consider the time-dependent single-particle Hamiltonian

$$h(t) = \frac{\mathbf{p}^2}{2m} + V(\mathbf{r}, t) \quad (3.66)$$

and the corresponding Schrödinger equation

$$h(t)\psi(t) = i\hbar \frac{\partial}{\partial t} \psi(t). \quad (3.67)$$

Introducing spherical coordinates  $r, \theta, \phi$  with respect to the axis  $\omega$ , we can represent the time-dependence of  $V(t)$  in the following way. If  $V(\mathbf{r}, 0)$  is the

potential at time  $t = 0$ , then we have at time  $t$ :

$$V(\mathbf{r}, t) = V(r, \theta, \varphi - \omega t, 0). \quad (3.68)$$

Again we realize that  $V$  is only time dependent if it depends on  $\varphi$ . In other words,  $V$  should not have axial symmetry around the rotational axis, because then there can be no collective rotation possible around an axis of symmetry for a quantum mechanical system (see Sec. 1.5.1). Because of the very simple time dependence of  $V(t)$  in Eq. (3.68), a unitary transformation exists which eliminates this time dependence. It is

$$U = e^{i\omega t} \quad (3.69)$$

with  $\omega \cdot \mathbf{l} = (\hbar/i)\omega \cdot \partial/\partial\varphi$ .  $U$  produces a rotation of an angle  $\omega t$  around the rotational axis  $\omega$ .

We find the time-dependent operator

$$Uh(t)U^{-1} = h(0) \quad (3.70)$$

and define

$$\tilde{\psi} = U\psi, \quad (3.71)$$

with

$$i\hbar\dot{\tilde{\psi}} = i\hbar U\dot{\psi} + i\hbar\dot{U}\psi = (h(0) - \omega l)\tilde{\psi}. \quad (3.72)$$

Equation (3.72) is a time-dependent Schrödinger equation with an explicitly time-independent effective Hamiltonian  $h_\omega$ . It thus can be solved as an eigenvalue problem in the standard way:

$$h_\omega\tilde{\psi} = (h(0) - \omega l)\tilde{\psi} = \epsilon'_\omega\tilde{\psi}, \quad (3.73)$$

where  $\epsilon'_\omega$  are eigenvalues of the effective Hamiltonian. To get the energies of the original Hamiltonian, we have to calculate

$$\epsilon_\omega = \langle \psi | h(t) | \psi \rangle = \langle \tilde{\psi} | h(0) | \tilde{\psi} \rangle = \epsilon'_\omega + \omega \langle \tilde{\psi} | \mathbf{l} | \tilde{\psi} \rangle. \quad (3.74)$$

The term  $\omega l$  is usually called the Coriolis term.

We have now solved the time-dependent Schrödinger equation in a rotating potential and found that we must diagonalize an effective time-independent Hamiltonian. We want to emphasize that we have not derived a priori the Hamiltonian as it is seen from the rotating coordinate system, since we transformed only the coordinates and not the momenta. In fact, in the case of pure translational motion, we would get a similar result [ $h_\omega = h(0) - \mathbf{v} \cdot \mathbf{p}$ ], but from Galilean invariance we require that the Hamiltonian seen from the moving coordinate system is the same as in the rest frame. Nevertheless, it turns out that in the special case of rotations,  $h_\omega$  in Eq. (3.73) is identical with the Hamiltonian as seen from the rotating system [Va 56; Br 64, p. 69]. From the term  $\omega l$ , we can derive the Coriolis force as well as the centrifugal force.

For systems with spin the operator which generates rotations is  $\mathbf{j} = \mathbf{l} + \mathbf{s}$ . The orientation of the rotational axis is usually chosen as parallel to the  $x$ -axis because it is understood to be perpendicular to the axis of symme-

try, which for  $\omega=0$  is the  $z$ -axis. For higher angular momenta, one also investigates nonsymmetric single-particle potentials. Nevertheless, we require that  $\omega$  is parallel to a principal axis of the potential. Therefore, the many-body Hamiltonian of the cranking model is given by ( $J_x = \sum_{i=1}^A j_x^{(i)}$ ):

$$H_\omega = H - \omega J_x = \sum_{i=1}^A h_\omega^{(i)}, \quad (3.75)$$

where  $H$  is a sum of deformed single-particle Hamiltonians.

Within the cranking model we must now diagonalize  $H_\omega$ , and the resulting ground state wave function  $\Phi_\omega$  is a Slater determinant. As in the normal shell model (with  $\omega=0$ ) the question arises how the levels in the single-particle potential should be filled to obtain the lowest energy state for any given angular momentum (the yrast level). The answer to this question (given in Sec. 11.4) is that we have to minimize the energy  $E' = \langle \Phi | H - \omega J_x | \Phi \rangle$ , that is, we have to fill up the potential in the usual way *in the rotating frame*.

For the energy in the laboratory system, from Eq. (3.74) we get

$$E(\omega) = \langle \Phi_\omega | H | \Phi_\omega \rangle = \langle \Phi_\omega | H_\omega | \Phi_\omega \rangle + \omega \langle \Phi_\omega | J_x | \Phi_\omega \rangle. \quad (3.76)$$

Since  $E(\omega)$  cannot depend on the sign of  $\omega$ , one finds

$$E(\omega) = E(0) + \frac{1}{2} g_1 \omega^2 + \dots \quad (3.77)$$

and, since for  $\omega=0 \langle \Phi_0 | J_x | \Phi_0 \rangle = 0$ ,

$$J(\omega) = \langle \Phi_\omega | J_x | \Phi_\omega \rangle = g_2 \omega + \dots \quad (3.78)$$

We can show that the constants  $g_1$  and  $g_2$  are equal [Sch 61],

$$g_1 = g_2, \quad (3.79)$$

using the fact that  $E(\omega)$  is the lowest eigenvalue of  $H_\omega$ . According to the variation principle of Ritz, we get  $\Phi_\omega$  as a solution of the equation

$$\delta \langle \Phi | H - \omega J_x | \Phi \rangle = 0, \quad (3.80)$$

where  $|\Phi\rangle$  is any one from the family of all possible Slater determinants. The condition is also fulfilled if we take  $|\Phi\rangle$  to be taken out of the set  $\{\Phi_\omega\}$ , where  $\Phi_\omega$  is an eigenfunction of  $H - \omega' J_x$ , and  $\omega'$  runs through all real numbers. Then we find from Eq. (3.80):

$$\frac{d}{d\omega'} \langle \Phi_\omega | H | \Phi_\omega \rangle - \omega \frac{d}{d\omega'} \langle \Phi_\omega | J_x | \Phi_\omega \rangle = 0 \quad (3.81)$$

or

$$g_1 = \frac{1}{\omega} \frac{d}{d\omega} E(\omega) \Big|_{\omega=0} = \frac{d}{d\omega} J(\omega) \Big|_{\omega=0} = g_2.$$

We also derive from Eq. (3.80):

$$\omega = \frac{dE}{dJ}. \quad (3.82)$$

To have a comparison with experiment, we have to determine the value of

the angular velocity. Inglis [In 54] proposed to include the zero-point oscillations at least semiclassically by requiring

$$J = \langle \Phi_\omega | J_x | \Phi_\omega \rangle = \sqrt{I(I+1)}. \quad (3.83)$$

In first order we get

$$\omega = \frac{\sqrt{I(I+1)}}{g_1} \quad (3.84)$$

and, from (3.77),

$$E(I) = E(0) + \frac{1}{2g_1} I \cdot (I+1). \quad (3.85)$$

For higher  $\omega$ -values there are deviations from this  $I(I+1)$  law. In general, the moment of inertia is defined as

$$g = \frac{J}{\omega}. \quad (3.86)$$

Up to now we have investigated only completely independent particle motion, by which we mean that we have even neglected the influence of the rotation on the average field. In Section 7.7 we will show how this can be taken into account.

### 3.4.2 The Cranking Formula

In the case of a pure  $I(I+1)$  spectrum, we need calculate only one constant, the *moment of inertia*. It is already determined by the  $2^+$  state and therefore it seems meaningful to apply perturbation theory for such small  $I$ -values.

We start with the unperturbed system of a deformed potential, which is filled up to the Fermi level. Levels below will be called holes (indices  $i, i', \dots$ ); levels above will be called particles (indices  $m, m', \dots$ ). The shell model basis consists of the ground state  $|\Phi_0\rangle$ ,  $ph$ -states  $|mi\rangle = a_m^+ a_i |\Phi_0\rangle$ ,  $2p-2h$  states, and so on. The perturbation  $\omega \cdot J_x$  is a one-particle operator and can therefore excite only one  $ph$  pair at a time. Therefore, we get for the perturbed wave function up to first order

$$|\Phi\rangle = |\Phi_0\rangle + \omega \sum_{im} \frac{\langle mi | J_x | \Phi_0 \rangle}{\epsilon_m - \epsilon_i} a_m^+ a_i |\Phi_0\rangle, \quad (3.87)$$

where  $\epsilon_i$  and  $\epsilon_m$  are the single-particle energies of the Hamiltonian  $H$ . The expectation value of  $J_x$  up to first order in  $\omega$  is then

$$J = \langle \Phi | J_x | \Phi \rangle = 2\omega \sum_{im} \frac{|\langle mi | J_x | \Phi_0 \rangle|^2}{\epsilon_m - \epsilon_i}, \quad (3.88)$$

which, together with (3.78) gives for the moment of inertia\*

$$g_{\text{Inglis}} = 2 \cdot \sum_{mi} \frac{|\langle mi | J_x | i \rangle|^2}{\epsilon_m - \epsilon_i}. \quad (3.89)$$

\* In molecular physics a similar formula has been derived by Wick [Wi 48].

This is the well known *Inglis formula* for the moment of inertia [In 54, BM 55].

The moments of inertia that result from this formula are usually very close to the rigid body value of the moment of inertia [Eq. (1.49)]. In fact, we shall see in Section 3.4.3 that, in the case of a pure anisotropic oscillator, this will be an exact result. Lüders [Lü 60] showed that this is the result for any independent particle model in the limit of large particle numbers (see also [AB 59, Ro 59, SB 64, Da 75, KG 78]).

We can understand this result qualitatively, if we realize that the velocity distribution of the ground state in a deformed static potential is nearly isotropic (see Sec. 13.3), and that this fact is not changed in the rotating system by Coriolis or centrifugal forces (see [BJ 76b]). Then there is no net flow in the intrinsic system and from the laboratory frame we observe a rigid-rotation velocity distribution.

As we have seen in Section 1.5.1, the experimental moments of inertia are a factor of 2 to 3 smaller than their rigid body values. Bohr and Mottelson [BM 55, Mo 56] already indicated that residual two-body interactions would lower these values. The most important influences in this respect are the correlations of the pairing type. Since they can be included very easily within the BCS-formalism (see Chap. 6) in a single-particle description, we give here the derivation of the so-called Belyaev formula [Be 59, 61], which is the extension of the Inglis formula (3.89) that includes pairing correlations. (Readers not familiar with this formalism are referred to Chapter 6.)

In this case,  $|BCS\rangle$  represents the BCS-ground state (6.31) and excitations are given by the two-quasi-particle states  $\alpha_k^+ \alpha_{k'}^- |BCS\rangle$ , four-quasi-particle states, etc. By analogy with Eq. (3.87), we obtain the perturbed wave function

$$|\Phi\rangle = |BCS\rangle + \omega \sum_{k < k'} \frac{\langle BCS | \alpha_k^- \alpha_{k'}^+ J_x | BCS \rangle}{E_k + E_{k'}} \alpha_k^+ \alpha_{k'}^- |BCS\rangle, \quad (3.90)$$

where  $E_k + E_{k'}$  is the excitation energy of the quasi-particle pair  $k, k'$ . The quasi-particle energies are given by

$$E_k = \sqrt{(\epsilon_k - \lambda)^2 + \Delta_k^2}. \quad (3.91)$$

Proceeding as in Eqs. (3.88) and (3.89), we find for the moment of inertia

$$\mathfrak{J}_{\text{Belyaev}} = 2 \sum_{k < k'} \frac{|J_{x_{kk'}}^{(2)}|^2}{E_k + E_{k'}}. \quad (3.92)$$

From Eq. (E.16), we find  $J_x^{(2)}$  and get

$$\mathfrak{J}_{\text{Belyaev}} = 2 \sum_{k, k' > 0} \frac{|\langle k | J_x | k' \rangle|^2}{E_k + E_{k'}} (u_k v_{k'} - u_{k'} v_k)^2. \quad (3.93)$$

This formula for the moment of inertia indeed yields lower values as compared to expression (3.89). Two effects are responsible for this:

- (i) The energy denominator is much larger than the particle-hole energies in Eq. (3.89). The parameter  $\Delta$  [Eq. (3.91)] produces a gap of at least  $2\Delta \approx 2$  MeV for the important levels in the neighborhood of the Fermi surface
- (ii) The factor  $(u_k v_{k'} - u_{k'} v_k)^2$  is usually somewhat smaller than unity.

The lowering of the moment of inertia in the BCS-theory, as compared to the rigid body value, corresponds to a superfluid slippage of some nucleons as the nucleus rotates [Mi 59, 60].

Extended numerical calculations [GR 60, NP 61, MT 75] for realistic nuclei show a remarkable agreement with the experimental values. As we shall see in the next section, it is very important to apply the Inglis or the Belyaev formula to self-consistent wave functions, that is, those calculated at deformations that correspond to the energy minimum. In most of these calculations, this is achieved by using Nilsson wave functions and energies at the experimentally observed deformations as well as the experimentally determined values of the gap  $\Delta$  (see also [MN 59]).

The success of these calculations, which produce roughly correct moments of inertia lying between the (too small) irrotational values and the (too large) rigid body value gives us great confidence that the picture of rotational nuclei as a deformed superfluid many-body system is correct.

Of course, we can investigate the influence of the *residual interaction* on the moment of inertia. This can be done within the framework of linear response theory (see Sec. 8.5.3 and [MSV 72]). In this kind of theory, the external field represented by the Coriolis operator  $J_x$  can excite virtual vibrations of the core which, in turn, have an influence on the moment of inertia. There are two types of such vibrations: surface oscillations (*ph* vibrations), which correspond to the stretching effect, and oscillations in the pairing correlations (*pp*-vibrations; see Sec. 8.3.5). The net result of such calculations is that both effects more or less cancel, and we get roughly the same values for the moments of inertia (Fig. 3.14) as given by the BCS theory.

We have now discussed the application of perturbation theory to the calculation of the expectation value of  $J_x$ , that is, the moment of inertia. In a similar fashion, we can calculate other properties of the rotating nucleus, for example, the *gyromagnetic ratio*  $g_R$  or the magnetic moment of the first  $2^+$  state. Since the magnetic moment  $\mu$  is defined as the expectation value of  $\mu_z$  in the state  $|I, M=I\rangle$  [Eq. (B.31)] and the cranking model wave functions are not eigenfunctions of angular momentum, it is not clear at this point how to calculate  $\mu$ . In Sec. 11.4, we will see that a projection technique has to be applied. In lowest order, we get a very simple result, which can be understood easily within the semiclassical picture of the cranking model:

$$\mu = \langle \Phi_\omega | \mu_x | \Phi_\omega \rangle. \quad (3.94)$$

We can therefore define the gyromagnetic ratio (1.37) by

$$\mu = g_R \cdot J = g_R \cdot \langle \Phi_\omega | J_x | \Phi_\omega \rangle. \quad (3.95)$$

From (3.90), in first order perturbation theory, we get

$$g_R = \frac{1}{\beta} \sum_{k, k' > 0} \frac{\langle \langle k | J_x | k' \rangle \langle k' | \mu_x | k \rangle + c.c.)}{E_k + E_{k'}} (u_k v_{k'} - u_{k'} v_k)^2. \quad (3.96)$$

The values calculated with these formulae are smaller than the liquid drop value  $g_R = Z/A$  [Eq. (1.37)] and agree quite well with the experimental data [MSV 72].

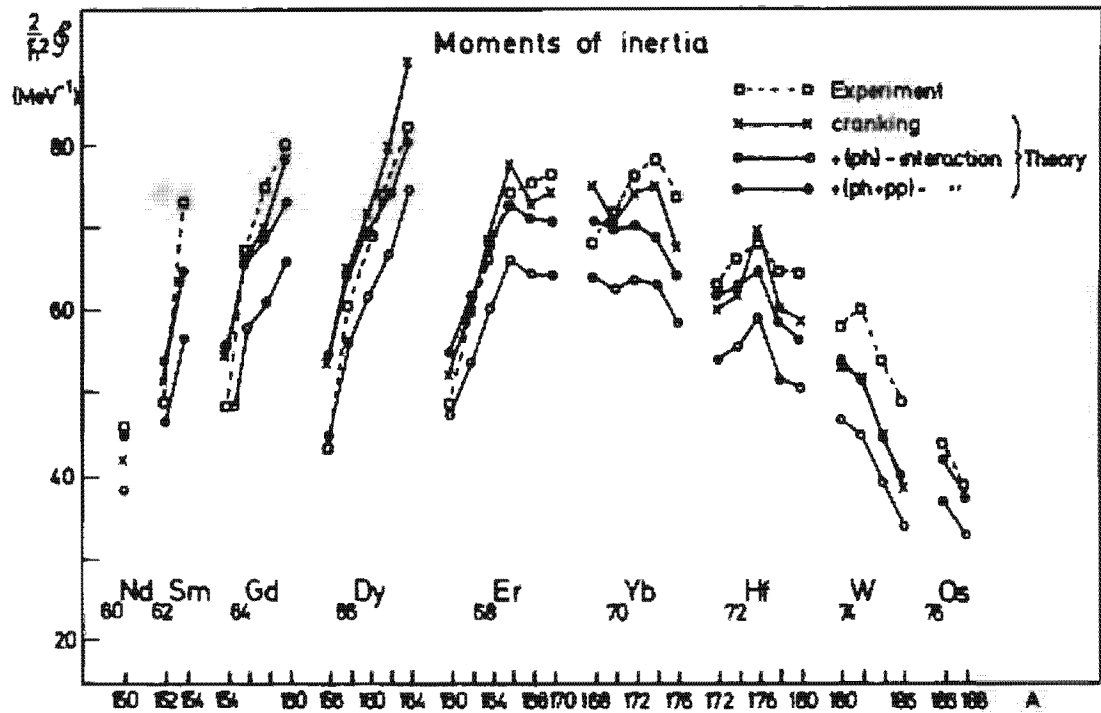


**Figure 3.14.** Moments of inertia in rare earth nuclei. The squares indicate experimental values [NP 61]; the crosses are obtained from the Belyaev formula (3.93). The open circles take into account only the stretching effect ( $ph$  interaction); in addition to that, the closed circles also take into account the antipairing effect ( $pp$ -interaction). (From [MSV 72].)

As we have seen in Section 3.2, deviations from the  $I(I+1)$  law occur as we go to higher angular momenta. To calculate the  $B$  and  $C$  coefficients [Eq. (3.1)] connected with these deviations, one has used perturbation theory in higher order, including the effects of a residual interaction [Ma 65, Ma 67a, MR 70], so that the most important effect is the so-called Coriolis-antipairing effect, which we will discuss in Section 7.7. As we shall see, it is only at the very high spin states with  $I > 30$  or 40 that one can expect the pairing correlations to vanish.

### 3.4.3 The Rotating Anisotropic Harmonic Oscillator

We have seen in Section 2.8.3 that the anisotropic harmonic oscillator can be solved analytically and that it provides at least a qualitative model for a deformed nucleus. It turns out that it can also be solved analytically in the rotating frame (see [Va 56, Ze 75, RBK 75, GMZ 78]), because  $I_x = yp_z - zp_y$  is a quadratic form in the coordinates  $x, y, z$  and momenta  $p_x, p_y, p_z$ .

We can forget about the spin, since the potential does not depend on it (the term  $-\omega s_x$  in the Coriolis operator can be diagonalized separately in the spin space and gives only a diagonal contribution). The Hamiltonian then has the form

$$h_\omega = -\frac{\hbar^2}{2m}\Delta + \frac{1}{2}m(\omega_x^2x^2 + \omega_y^2y^2 + \omega_z^2z^2) - \omega(yp_z - zp_y). \quad (3.97)$$

We introduce the creation and annihilation operators for the harmonic oscillator

bosons in  $x$ ,  $y$ , and  $z$  directions  $a_x$ ,  $a_y$ , and  $a_z$ :

$$\begin{aligned} x &= \left( \frac{\hbar}{2m\omega_x} \right)^{\frac{1}{2}} (a_x + a_x^+) \quad p_x = \frac{\hbar}{i} \left( \frac{m\omega_x}{2\hbar} \right)^{\frac{1}{2}} (a_x - a_x^+), \\ y &= i \left( \frac{\hbar}{2m\omega_y} \right)^{\frac{1}{2}} (a_y - a_y^+) \quad p_y = \hbar \left( \frac{m\omega_y}{2\hbar} \right)^{\frac{1}{2}} (a_y + a_y^+), \\ z &= \left( \frac{\hbar}{2m\omega_z} \right)^{\frac{1}{2}} (a_z + a_z^+) \quad p_z = \frac{\hbar}{i} \left( \frac{m\omega_z}{2\hbar} \right)^{\frac{1}{2}} (a_z - a_z^+). \end{aligned} \quad (3.98)$$

In these operators,  $\hbar\omega$  is of the form

$$\begin{aligned} \hbar\omega &= \hbar\omega_x \left( a_x^+ a_x + \frac{1}{2} \right) + \hbar\omega_y \left( a_y^+ a_y + \frac{1}{2} \right) + \hbar\omega_z \left( a_z^+ a_z + \frac{1}{2} \right) \\ &\quad + \frac{\hbar\omega}{2\sqrt{\omega_x\omega_y}} \{ (\omega_y - \omega_z)(a_y^+ a_z^+ + a_y a_z) + (\omega_y + \omega_z)(a_y^+ a_z + a_z^+ a_y) \}. \end{aligned} \quad (3.99)$$

The Coriolis operator in (3.99) has two contributions. The first one creates or annihilates two oscillator quanta. Therefore, it couples shells with major quantum numbers  $N$  and  $N \mp 2$ .\* The second part conserves the total number of quanta, but shifts quanta from the  $y$ -direction into the  $z$ -direction and vice versa.

**3.4.3.1 The Inglis Formula.** First we want to treat the Coriolis term in perturbation theory. In the Inglis formula (3.89), the  $\Delta N = \pm 2$  part has the energy denominator  $\pm \hbar(\omega_y + \omega_z)$  and the  $\Delta N = 0$  part has the denominator  $\pm \hbar(\omega_y - \omega_z)$ . The matrix elements of  $a, a^+$  are given in Eq. (C. 12f),

$$\langle n - l | a | n \rangle = \sqrt{n}, \quad \langle n + l | a^+ | n \rangle = \sqrt{n+1},$$

and we get, from (3.89)

$$g_{\text{Inglis}} = \frac{\hbar}{2\omega_y\omega_z} \left\{ \frac{(\omega_y - \omega_z)^2}{\omega_y + \omega_z} (N_y + N_z) + \frac{(\omega_y + \omega_z)^2}{\omega_y - \omega_z} (N_z - N_y) \right\}, \quad (3.100)$$

where the

$$N_{x, y, z} = \sum_{i=1}^A \left( a_{x, y, z}^+ + \frac{1}{2} \right), \quad (3.101)$$

satisfy the relations

$$\bar{x}^2 = \frac{1}{A} \sum_{i=1}^A \langle x^2 \rangle_i = \frac{1}{A} \frac{\hbar}{m\omega_x} \sum_{i=1}^A \left( n_x + \frac{1}{2} \right)_i = \frac{\hbar}{Am\omega_x} \cdot N_x. \quad (3.102)$$

Very important for the following discussion is the *self-consistency condition*, [BM 75], namely, that the potential (given by  $\omega_x, \omega_y, \omega_z$ ) has the same shape as the density distribution (given by  $\bar{x}^2, \bar{y}^2$  and  $\bar{z}^2$ ):

$$\sqrt{\bar{x}^2} : \sqrt{\bar{y}^2} : \sqrt{\bar{z}^2} = \frac{1}{\omega_x} : \frac{1}{\omega_y} : \frac{1}{\omega_z}. \quad (3.103)$$

Together with Eq. (3.102), we find

$$\omega_x N_x = \omega_y N_y = \omega_z N_z = C. \quad (3.104)$$

\* It vanishes for small deformations ( $\omega_y \approx \omega_z$ ) and is therefore often neglected [ALL 76].

With this condition we can rewrite Eq. (3.100):

$$g_{\text{ring}} = \hbar \left( \frac{N_y}{\omega_y} + \frac{N_z}{\omega_z} \right). \quad (3.105)$$

The value of the moment of inertia so obtained is identical to the rigid body value. From Eq. (3.102) we get

$$g^{\text{rig}} = m \sum_{i=1}^A (\langle y^2 \rangle_i + \langle z^2 \rangle_i) = \hbar \left( \frac{N_y}{\omega_y} + \frac{N_z}{\omega_z} \right). \quad (3.106)$$

Once again, we would like to stress the point that the self-consistency condition (3.104) is crucial for this result. If we occupied the  $y$ - and  $z$ -direction with the same number of oscillator quanta ( $N_y = N_z$ ), we would get from Eqs. (3.100) and (3.102) a value

$$g = \hbar \frac{(N_y/\omega_y - N_z/\omega_z)^2}{(N_y/\omega_y + N_z/\omega_z)} = Am \frac{(\bar{y}^2 - \bar{z}^2)^2}{\bar{y}^2 + \bar{z}^2}, \quad (3.107)$$

which is proportional to the irrotational flow value [BM 75].

**3.4.3.2 Exact Solution.** In the next step, we go beyond perturbation theory and diagonalize the single-particle Hamiltonian (3.99) exactly.\* It is a quadratic form in the boson operators  $a, a^*$  and can therefore be diagonalized [RBK 75] in the same way as one diagonalizes quadratic forms of the RPA-type (see Chap. 8).

To diagonalize the single-particle Hamiltonian, we introduce a canonical transformation among the momenta  $p_y, p_z$  and the coordinates  $y, z$  [Va 56]:

$$\begin{aligned} Q_2 &= \alpha_2(y + \beta p_z), \\ Q_3 &= \alpha_3(z + \beta p_y), \\ P_2 &= \alpha_2^{-1}(1 - \delta\beta)^{-1}(p_y + \delta z), \\ P_3 &= \alpha_3^{-1}(1 - \delta\beta)^{-1}(p_z + \delta y), \end{aligned} \quad (3.108)$$

which guarantees that the  $Q_i, P_i$  fulfill the commutation relations of momenta and coordinates. The constants  $\beta$  and  $\delta$  are determined by the requirement that the Hamiltonian (3.97) contains no mixed terms  $P_2 Q_3$  or  $P_3 Q_2$  in the new representation. The constants  $\alpha_2$  and  $\alpha_3$  normalize the new coordinates in such a way that the mass parameter is again  $m$ . In the new variables, the Hamiltonian has the form [Va 56]

$$h_\omega = \left( -\frac{P_x^2}{2m} + \frac{1}{2}m\omega_x^2 x^2 \right) + \left( -\frac{P_2^2}{2m} + \frac{1}{2}m\Omega_2^2 Q_2^2 \right) + \left( -\frac{P_3^2}{2m} + \frac{1}{2}m\Omega_3^2 Q_3^2 \right). \quad (3.109)$$

The coordinates  $x, Q_2, Q_3$  are the normal coordinates of the problem, and the frequencies  $\Omega_i$  are given by

$$\Omega_{2,3}^2 = \omega^2 + \omega_\pm^2 \pm \sqrt{\omega_-^4 + 4\omega^2\omega_+^2}, \quad (3.110)$$

with

$$\omega_\pm^2 = \frac{1}{2}(\omega_y^2 \pm \omega_z^2). \quad (3.111)$$

\* For the calculation of matrix elements in this rotating oscillator basis, see [LR 77].

We can now define rotating bosons  $B_2^+$ ,  $B_3^+$  in analogy to Eq. (3.98):

$$B_2^+ = (2\hbar m\Omega_2)^{-\frac{1}{2}}(P_2 + im\Omega_2 Q_2), \quad (3.112)$$

$$B_3^+ = -i(2\hbar m\Omega_3)^{-\frac{1}{2}}(P_3 + im\Omega_3 Q_3),$$

and obtain for the Hamiltonian

$$h_\omega = \hbar\omega_x \left( a_x^+ a_x + \frac{1}{2} \right) + \hbar\Omega_2 \left( B_2^+ B_2 + \frac{1}{2} \right) + \hbar\Omega_3 \left( B_3^+ B_3 + \frac{1}{2} \right). \quad (3.113)$$

The corresponding eigenstates

$$|n_x, n_2, n_3\rangle \propto (a_x^+)^{n_x} (B_2^+)^{n_2} (B_3^+)^{n_3} |-\rangle \quad (3.114)$$

are characterized by the numbers of rotating bosons.

Their single-particle energies are

$$\epsilon_{n_x, n_2, n_3} = \hbar\omega_x \left( n_x + \frac{1}{2} \right) + \hbar\Omega_2 \left( n_2 + \frac{1}{2} \right) + \hbar\Omega_3 \left( n_3 + \frac{1}{2} \right). \quad (3.115)$$

Assuming again a fixed occupation in a Slater determinant  $|-\rangle$ , that is, a fixed set of numbers  $N_x, N_2, N_3$  defined in analogy to Eq. (3.101) for rotating bosons, we find for the total energy in the rotating frame,

$$E'(\omega) = \langle H_\omega \rangle = N_x \hbar\omega_x + N_2 \hbar\Omega_2 + N_3 \hbar\Omega_3. \quad (3.116)$$

Remembering that  $\langle H_\omega \rangle$  is stationary with respect to variations of the eigenfunctions, we can calculate the expectation value of the angular momentum [RBK 75].

$$\langle L_x \rangle = -\langle \frac{\partial H_\omega}{\partial \omega} \rangle = -\frac{\partial}{\partial \omega} E' = \omega \left\{ \frac{4\omega_x^2}{\Omega_2^2 - \Omega_3^2} \left( \frac{N_3}{\Omega_3} - \frac{N_2}{\Omega_2} \right) - \left( \frac{N_2}{\Omega_2} + \frac{N_3}{\Omega_3} \right) \right\} \quad (3.117)$$

and the shape parameters  $x^2, y^2, z^2$ ,

$$x^2 = \langle x^2 \rangle = \frac{1}{m\omega_x} \langle \frac{\partial H_\omega}{\partial \omega_x} \rangle = \frac{1}{m\omega_x} \frac{\partial E'}{\partial \omega_x}, \quad y^2 = \dots, \quad (3.118)$$

and so on. The moment of inertia is given by

$$I = \frac{\langle L_x \rangle}{\omega} = m \langle y^2 + z^2 \rangle + \frac{4\hbar}{\Omega_2^2 - \Omega_3^2} (N_3 \Omega_3 - N_2 \Omega_2). \quad (3.119)$$

For the final construction of the many-body Slater determinant, however, we have to fix the occupation numbers  $N_x, N_2, N_3$ .

In the nonrotating case, the numbers  $N_x, N_y, N_z$  were determined by the self-consistency condition (3.104). It can be motivated by different arguments, which all give the same results at  $\omega=0$ . For  $\omega \neq 0$  this is no longer the case. Several methods have been proposed:

- (i) *Minimizing the expectation value  $E'(\omega)$  in Eq. (3.116) for fixed occupation as a function of the deformation parameters  $\omega_x, \omega_y$  and  $\omega_z$ , and the frequency  $\omega$  under the constraint of constant volume ( $x^2, y^2, z^2 = \text{const.}$ ) and fixed angular momentum  $\langle L_x \rangle$  [St 78, TA 79].*

- (ii) *Requiring an isotropic velocity distribution in the rotating frame [RBK 75]. This is reasonable for heavy nuclei, where there are many level crossings and one has always filled up the lowest levels in the potential (see Sec. 13.3). We then get the modified self-consistency condition*

$$N_x \omega_x = N_2 \Omega_2 = N_3 \Omega_3. \quad (3.120)$$

It can be shown that under this condition the shape of the mass distribution (given by  $\bar{x}^2, \bar{y}^2, \bar{z}^2$ ) is proportional to the shape of the potential if one includes the centrifugal potential  $\frac{1}{2}m(\omega \times r)^2$ .

From Eq. (3.119) we see that the self-consistency condition (3.120) yields the rigid-body value for the moment of inertia\* at the actual deformation, which may change for large  $I$ -values.

### 3.4.4 The Rotating Nilsson Scheme

For realistic heavy nuclei, the pure harmonic oscillator is only of a limited importance, because it does not contain the drastic energy shift of high  $j$  shell orbitals due to the  $I \cdot s$  term. As we have seen in Section 3.3, they play a crucial role in the interpretation of rotational spectra in all heavy nuclei.

One therefore has extended the Nilsson model and added a Coriolis term  $-\omega j_x$  to the single-particle Hamiltonian (2.89) [ALL 76, RNS 78]:

$$h'(\omega) = h - \omega j_x \quad (3.121)$$

Figure 3.15 shows the qualitative behavior of some of the single-particle levels thus obtained as a function of  $\omega$ . It shows the following features.

- (i) At  $\omega=0$  are the usual Nilsson levels. They are twofold degenerate with respect to time reversal symmetry ( $\pm \Omega$ ). For  $\omega \neq 0$ , this symmetry is broken by the Coriolis term, and a split into two single levels is observed.
- (ii) The cranked Nilsson Hamiltonian is still invariant under a rotation of  $180^\circ$  around the  $x$ -axis, that is, the two levels belong to eigenstates of the operator

$$\mathcal{R}_x = e^{i\pi j_x} \quad (3.122)$$

with the eigenvalues  $r_x = \pm i$  ("signature" [Bo 76a, b]).

- (iii) Some levels show an extremely strong level splitting with increasing  $\omega$ . They belong to orbits with large  $j$ - and small  $\Omega$ -values (e.g.,  $1i_{13/2}, 660\frac{1}{2}, 651\frac{1}{2}, 642\frac{1}{2}$ ). They show strong  $\Omega$ -mixing and alignment along the  $x$ -axis (decoupled bands).
- (iv) For even nuclei at moderate angular velocities, however, pairing correlations, as discussed in Section 3.2.2. and 7.7, should be taken into account. They counteract the rotational alignment and try to keep the particles in pairwise occupied orbits. In a full microscopic description of the backbending effect, the pair correlations must be taken into account self-consistently (see Sec. 7.7).
- (v) For large frequencies, the alignment effect brings levels from higher major shells down into the neighborhood of the Fermi surface.

\* It has recently been shown [FR 76b] that electrons confined by a harmonic potential and submitted to a constant magnetic field are rotating uniformly around the axis formed by the field; this is the analogous effect to the rigid body value of the moment of inertia discussed here.

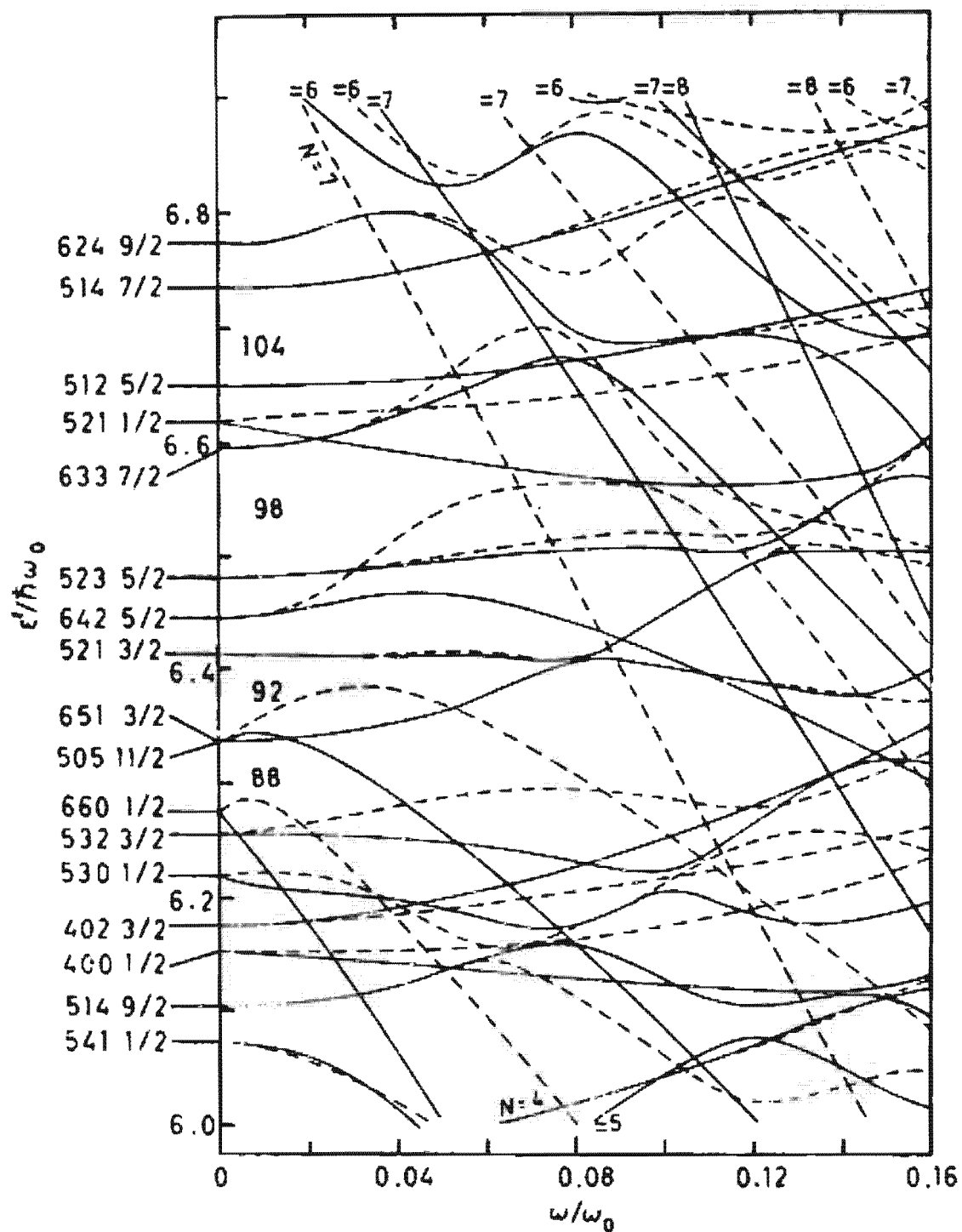


**Figure 3.15.** Qualitative behavior of the single-particle levels in a cranked Nilsson model at a prolate deformation ( $\delta = 0.25$ ) as a function of the cranking frequency  $\omega$  in units of  $\hbar\omega_0$ . Dashed lines correspond to levels with different  $r_x$ -quantum numbers. (We are grateful to Dr. R. Bengtsson for the preparation of this figure.)

- (vi) Eventually, new shell closures with new magic numbers develop at high angular momenta, which can influence the energy surface for the fission process (see Sec. 3.4.5).

### 3.4.5 The Deformation Energy Surface at High Angular Momenta

As we already discussed in Section 2.9, the pure Nilsson model cannot be used for the calculation of total energies nor for the calculation of the shape of the energy surfaces at large deformations, because the average part of the energy is not reproduced in a proper way within this model. Therefore, we calculate only the oscillating part of the deformation energy within this model and replace the smooth part by the liquid drop energy at the same deformation.

In the same way, we can calculate energy surfaces at a fixed angular momentum  $I$  as a function of the deformation. For an ellipsoidal shape [characterized by the parameters  $\beta$  and  $\gamma$  (Eq. 1.88)], the total energy is then given by

$$E(\beta, \gamma, I) = E_{\text{LDM}}(\beta, \gamma, I) + E_{\text{sh}}(\beta, \gamma, I) - \tilde{E}_{\text{sh}}(\beta, \gamma, I). \quad (3.123)$$

Here  $E_{\text{LDM}}$  is the deformation energy at a rotating ellipsoid with the rigid-body moment of inertia  $I_{\text{rig}}(\beta, \gamma)$ , because one assumes that at high angular momenta pairing correlations can be neglected.\*  $E_{\text{sh}}$  is the shell model energy and is obtained by summing up the single-particle energies.  $\tilde{E}_{\text{sh}}$  is the averaged part of it, and is calculated by an appropriate smoothing procedure (see Sec. 2.9).

There are two ways to derive these quantities from the diagonalization of a deformed single-particle potential in the rotating frame: Work either at constant frequency  $\omega$  [NPF 76] or at constant angular momentum  $I$  [ALL 76]. Both methods agree, if one uses a deformed Wood-Saxon potential, where the averaged moment of inertia is very close to the rigid-body value† [BJ 76b, NTP 77].

Several groups have carried out investigations along this line [BLL 75, NP 75, NPF 76, ALL 76, FDG 76, NTP 77] in many regions of the periodic table. Qualitatively they have found similar results:

- (i) For spherical or *weakly deformed nuclei* at the beginning of the rare earth region, the nuclei behave similarly to the classical liquid drop (Fig. 1.18): Up to angular momentum  $I = 50-70\hbar$  they are oblate and rotate around the symmetry axis. In this region, the rotation is

\* In fact, multiplicity measurement of the  $\gamma$ -cascade indicates the nucleus reaches the rigid-body moment of inertia at high spin values [SBC 76].

† The  $I^2$  term in the Nilsson potential (2.89) is non-local and gives contribution to the effective mass. It produces an averaged moment of inertia which is  $\sim 30-40\%$  larger than the rigid body value [Ty 70, 71, BR 71b, Je 73]. One has used scaling procedures to compensate for this effect [NTP 77].

not collective and one expects yrast traps (see Sec. 3.4.7). For higher  $I$ -values they rapidly change the shape to triaxial and prolate deformations (Jacobi-shapes; see Sec. 1.7). This transition corresponds to a drastic increase of the angular momentum ("giant backbending") as shown in Fig. 3.16. Finally, the nucleus fissions.

- (ii) Nuclei in the *middle of the rare earth region* start at low  $I$ -values at prolate shapes and rotate around an axis perpendicular to the symmetry axis. With increasing rotation the Coriolis force aligns more and more particles parallel to this axis, and at  $I \sim 40-50$  we find a transition to triaxial and sometimes even oblate shapes,\* as in Fig. 3.17. At very high angular momenta the nucleus again becomes triaxial and finally fission takes place.

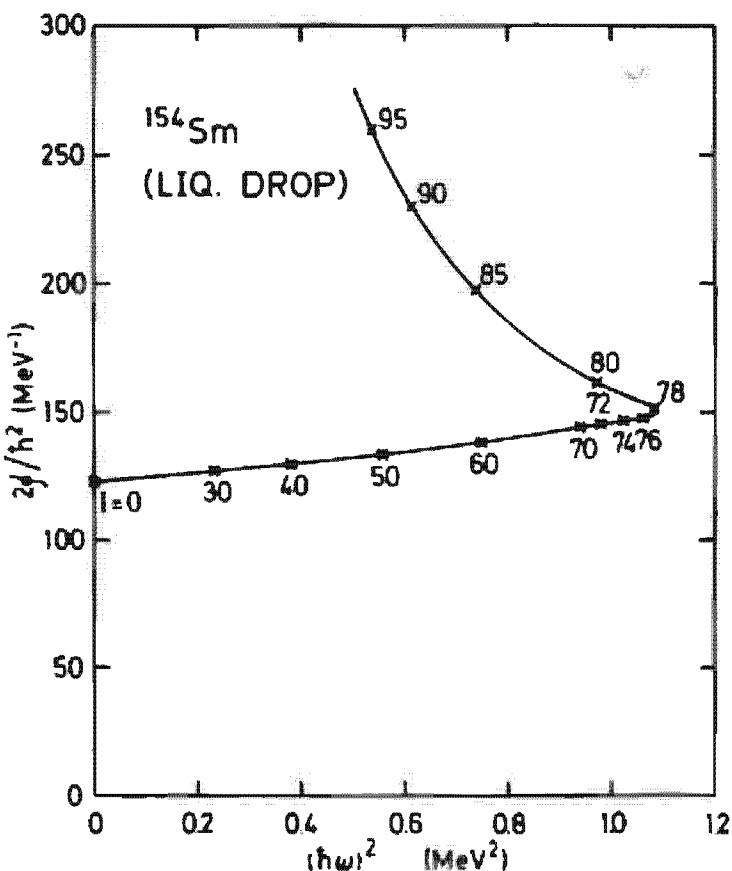
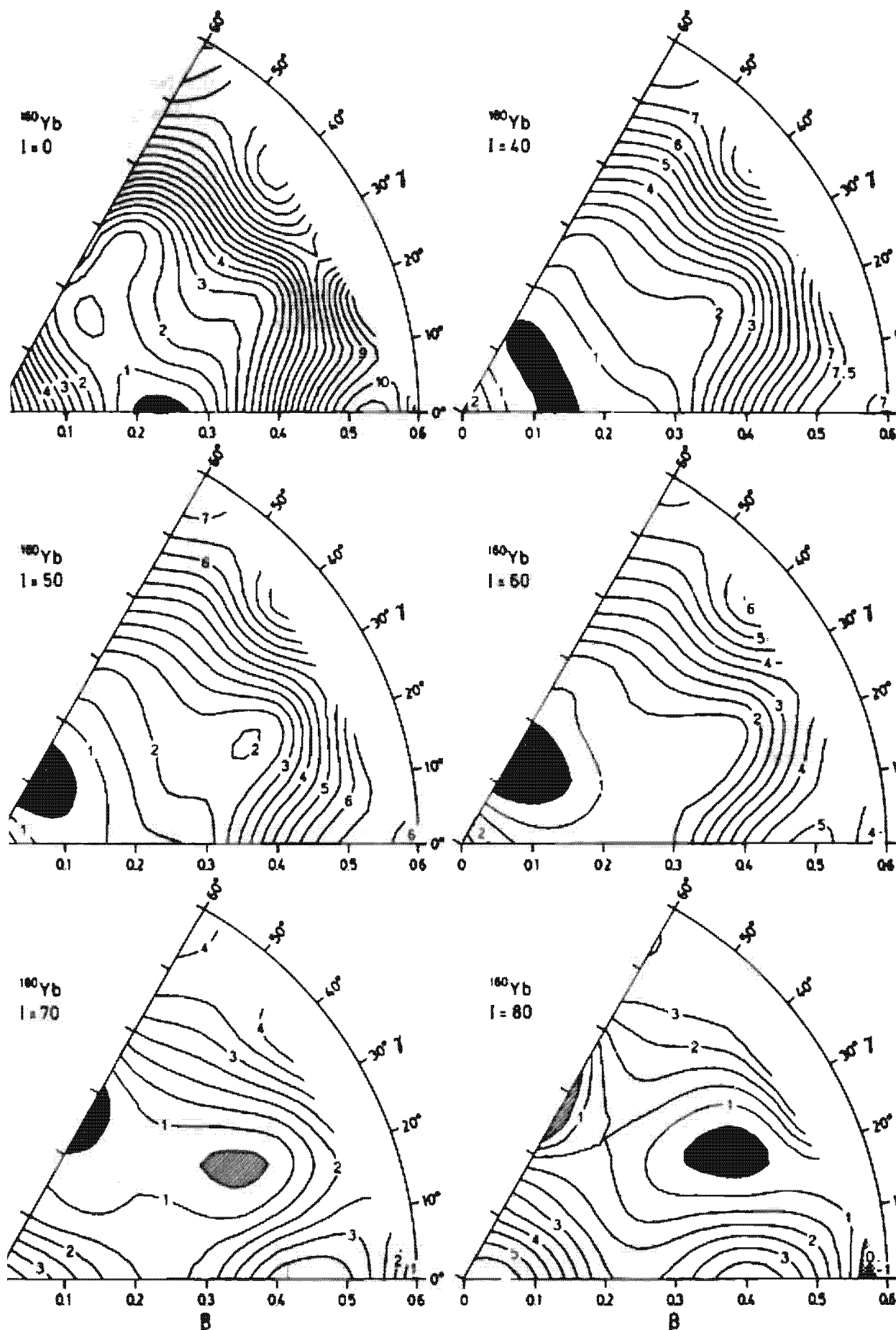


Figure 3.16. Backbending plot for the yrast spectrum of  $^{154}\text{Sm}$  in terms of the rotating liquid drop model. (From [ALL 76].)

We want to conclude this section with the remark that such calculations can only give a qualitative impression of the behavior of the nuclear many-body system at such high angular momenta. Only for very low excitations and for energy surfaces with deep minima can we expect the nucleus to have a fixed deformation. In general, it will carry out quantum mechanical zeropoint fluctuations around these minima which ought to be described by a dynamical theory (see, for instance, Chap. 10).

\* In calculations based on a Wood-Saxon potential [NTP 77], the nucleus does not reach such drastic  $\gamma$ -deformations, and fissions without having obtained an oblate shape.



**Figure 3.17.** Potential energy surfaces in the  $(\beta, \gamma)$  plane with inclusion of shell corrections for  $^{160}\text{Yb}$  as a function of angular momentum. (From [All 76]. Notice that these authors replace the Hill-Wheeler coordinate  $\gamma$  by  $-\gamma$ .)

### 3.4.6 Rotation about a Symmetry Axis

As we have seen in the last sections, there are regions in the periodic table where we find nuclei "rotating" around the symmetry axis. This happens in particular at the beginning and end of each major shell. At the beginning of each shell are a few particles sitting on a more or less spherical core. To create a large amount of angular momentum they all must align along the rotational axis (the  $x$ -axis), that is, classically speaking these particles have to run in the equatorial plane around the nucleus and produce an oblate density distribution.\*

Such a configuration is certainly not collective rotation, since there are only a few particles involved. Each single particle wavefunction is an eigenfunction of  $j_x$  with the eigenvalue  $\alpha_i$ . The component of the total angular momentum in the direction of the symmetry axis is given by

$$\langle J_x \rangle = \sum_{i=1}^A \alpha_i \quad (3.124)$$

To increase the angular momentum we have to change the occupation in the deformed well and to put particles from levels with lower (for instance negative)  $\alpha$ -values into those with higher (positive)  $\alpha$ -values.

Formally, this can be done again by a cranking procedure around the symmetry axis. Since the operator  $j_x$  commutes with  $h$ , we get the *single-particle energies in the "rotating frame."*

$$\epsilon'_i = \epsilon_i - \omega \alpha_i, \quad (3.125)$$

where  $\epsilon_i$  are the eigenvalues of  $h$  in the nonrotating frame. These are straight lines as a function of  $\omega$  (Fig. 3.18a) whose slope is given by

$$\frac{d\epsilon'_i}{d\omega} = -\alpha_i. \quad (3.126)$$

The condition to minimize the energy in the rotating frame

$$E' = \sum_{i=1}^A (\epsilon'_i - \omega \alpha_i) \quad (3.127)$$

guarantees that one always occupies the lowest levels  $\epsilon'_i$ . With increasing frequency  $\omega$  we thus obtain a stepwise increasing of the angular momentum (Fig. 3.18b). The distance between two steps and the size of the steps is given by the distances of the levels  $\epsilon_i$  and the angular momentum values  $\alpha_i$ . Therefore there is a statistical increase of the angular momentum with the frequency  $\omega$ . The *moment of inertia*  $\mathfrak{g}$  is defined only on the average (dashed line in Fig. 3.18b).

To get an estimate for the size of this moment of inertia [Bo 76b], we realize that each line in Fig. 3.18a has the slope  $-\alpha_i$  (increasing or

\* At the end of a major shell similar arguments can be applied for holes. We then end up with a rotation about the symmetry axis of a prolate density distribution. In the middle of a shell there are many valence particles forming a prolate deformed shape. It is easy to generate large angular momentum from a few alignment processes, without too drastic changes in deformation.

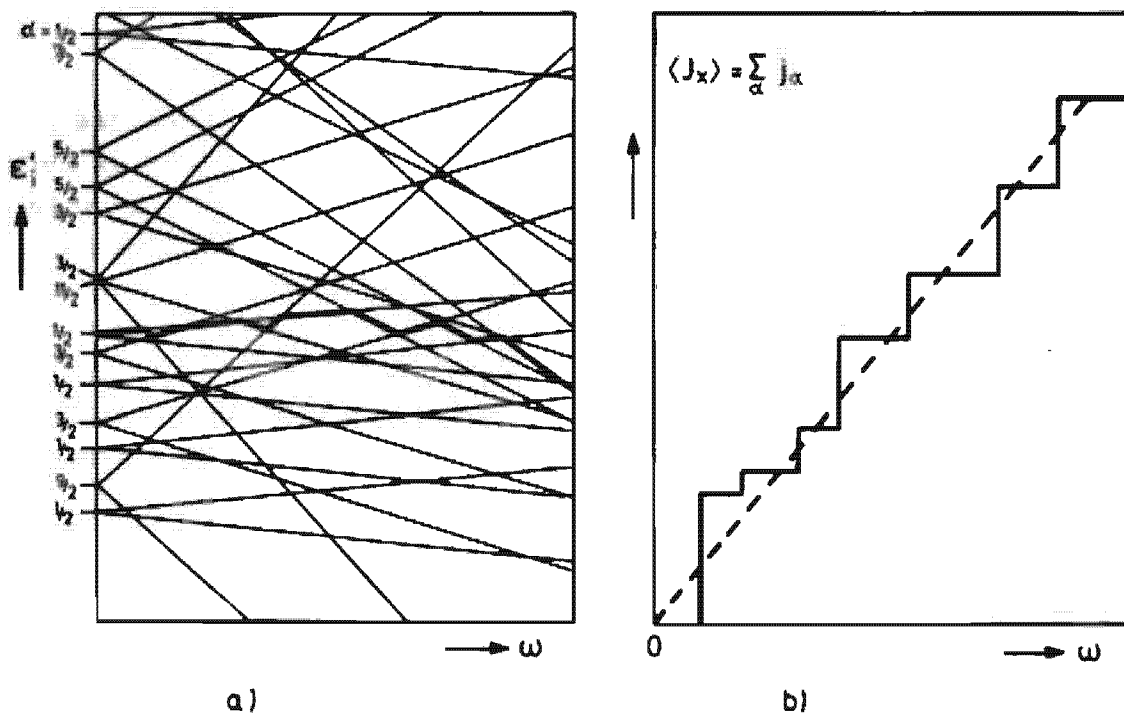


**Figure 3.18.** (a) Schematic representation of the eigenvalues  $\epsilon'$  in Eq. (3.125) as a function of the cranking frequency. (b) The angular momentum  $\langle J_x \rangle$  obtained by increasing values of  $\omega$  and by always occupying the lowest levels in (a).

decreasing, depending on the sign of  $\alpha$ ). For  $\omega=0$  the levels  $\pm\alpha$ , are all occupied pairwise. The resultant angular momentum vanishes. For finite  $\omega$  some of these levels with negative  $\alpha$  are no longer occupied, but other downward-coming levels with positive  $\alpha$ -values are occupied anew. For a fixed value of  $\alpha$  (for instance  $\alpha = \frac{1}{2}$ ) the number of newly occupied levels is on the average  $wag(\alpha)$ , where  $g(\alpha)$  is the density of levels with the quantum number  $\alpha$ . Therefore, we obtain for the angular momentum on the average

$$\langle J_x \rangle_{av} = \sum_{i \leq \epsilon_s} \alpha_i = \sum_{\alpha} \alpha \cdot \omega \cdot \alpha \cdot g(\alpha) = \omega \sum_{\alpha} \alpha^2 \cdot g(\alpha), \quad (3.128)$$

and for the average moment of inertia

$$g_{av} = \sum_{\alpha} \alpha^2 g(\alpha). \quad (3.129)$$

An evaluation of this quantity within the Thomas-Fermi approximation gives exactly the rigid-body value for the moment of inertia [Bo 76b]. On the average, "single-particle" rotation around the symmetry axis therefore shows quite a similar behavior to collective rotation, although the internal structure is completely different.

### 3.4.7 Yrast Traps

Since the level spacing in the case of a rotation around the symmetry axis has a statistical character, one expects *yrast traps* (high spin isomeric states). They are defined as yrast states which cannot undergo a rapid  $\gamma$ -transition and have been predicted by Bohr and Mottelson [IBM 74].

Filling the levels in the rotating well always from the bottom, we eventually obtain, with increasing angular velocity, jumps in the angular momentum by several units (see Fig. 3.18b). This can be visualized most easily in a representation of the eigenvalues  $\epsilon_i$  in the nonrotating oblate deformed Nilsson well as a function of the components  $\alpha$  of the angular momentum along the symmetry axis (Fig. 3.19). For small deformations we have rather pure  $j$ -configurations. The eigenvalues  $\epsilon_i$  for levels in the same  $j$ -shell lie on approximate parabolas [see Eq. (3.39); we have only to replace  $\Omega$  by  $\alpha$ ]. At oblate deformations ( $\beta < 0$ ) the highest  $\alpha$ -values, that is, the most aligned states, have the deepest energy, because their oblate density distribution in the equatorial plane has the maximal overlap with the oblate density of the core.

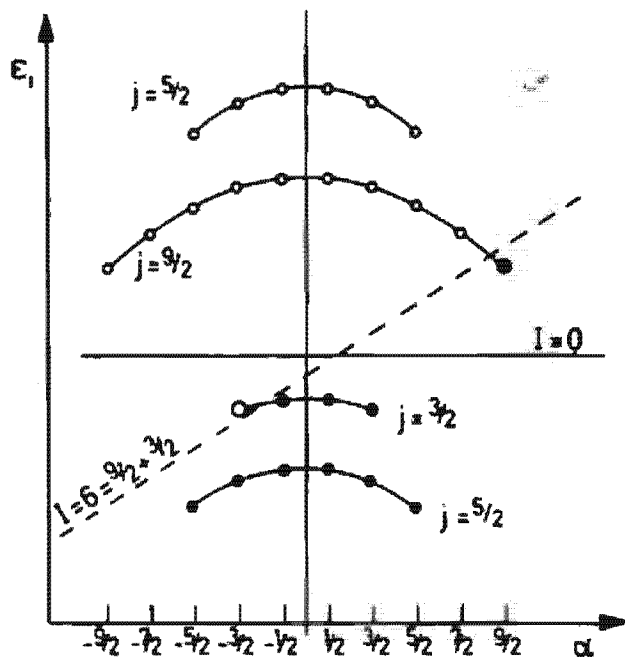


Figure 3.19. Schematic representation of the single-particle energies  $\epsilon_i$  in an oblate deformed Nilsson well as a function of  $\alpha$  (the eigenvalue of  $j_x$ ) with the Fermi surface at  $I = 0$  (full line) and at  $I = 6$  (dashed line).

At  $\omega = 0$ , the Fermi surface is a horizontal line and all levels below it are occupied. At finite  $\omega$ -values, according to Eq. (3.125), the Fermi level in the rotational frame has a slope  $\omega$ . As the value of  $\omega$  increases, levels with negative  $\alpha$ -values are vacated and those with positive  $\alpha$ -values are newly occupied. In Fig. 3.19 we show a situation where a jump of 6 units of angular momentum occurs. The remaining  $I$ -values on the yrast line can be obtained by constructing  $ph$ -configurations with respect to the rotated energy surface. This is usually connected with an increase in energy.

Therefore, it may happen that the yrast line is no longer a monotonically increasing function of  $I$ , and a certain level with  $I = I_0$  can have a deeper energy than the neighboring levels with  $I = I_0 - 1, I_0 - 2, \dots$ . A fast  $\gamma$  transition of  $E1$ -,  $E2$ -,  $M1$ - or  $M2$ -character (i.e., with low multipolarity; see Appendix B) is then not allowed (so-called *energy spin traps*).

Even if this is not the case, the internal structure of the states with  $I_0 - 1, I_0 - 2$  might be rather different from the structure of the state  $I_0$ . Then the transition matrix elements can be very small and the lifetime of the state  $I_0$  is very large (*structure spin traps*). Examples are cases where the states with  $I_0 - 1$  or  $I_0 - 2$  can only be reached from the state  $I_0$  by a  $2p-2h$  excitation, or cases where the  $\gamma$ -transition matrix element is hindered by the intrinsic selection rules of the single-particle wave functions (for instance,  $I$ -forbidden  $M1$ -transitions; see Sec. 2.7.2.).

Several groups have investigated the theoretical possibility of yrast traps by searching for cases of rotation around the symmetry axis in the energy surfaces at high angular momenta and by investigating the detailed single-particle structure in these cases [ALL 76, CDS 77, AK 77, DNM 77, PFL 78, PTF 78, AHL 78, Ab 78, MDN 78]. Some regions in the periodic table have been found in which they should be expected. These are mostly weakly deformed nuclei such as Te, Ba, Ce, Sm, neutron deficient rare earth isotopes, and nuclei in the Pb-region.

On the *experimental side* we have known for a long time about states with large angular momenta and very long lifetimes for spherical nuclei. These are states with rather pure high  $j$ -shell configurations, which have no allowed  $\gamma$ -transition matrix elements of low multipolarity to other states at deeper energy. The most famous example [PAG 62] is the  $18^+$  isomer in  $^{212}\text{Po}$  with a lifetime of 45 sec, which consists of an aligned  $(\pi h_{9/2})^2(\nu i_{11/2})^2$  configuration.

Another group of high spin isomers, usually called *K-isomers*, were observed in well deformed nuclei, such as the  $4s$  and the  $3ly$  isomers in  $^{178}\text{Hf}$ , which can be interpreted as a  $K'' = 8^-$  and a  $K'' = 16^+$  band head, whose  $\gamma$ -decay is *K*-forbidden [HR 68, KL 77].

Finally, in recent years an island of about 20 adjacent nuclei in the light rare earth region with long lived isomers has been found [PBB 77]. They are probably associated with oblate deformation and "single-particle" rotation [AHL 78].

The properties of nuclei in the vicinity of  $^{208}\text{Pb}$  have usually been studied in terms of the spherical shell model with residual interaction and a proper angular momentum coupling. Since these configurations are rather pure, some calculations of this type could explain measured excitation energies with extraordinary accuracy [BBH 77].

The physical reason for the aligned high spin configurations having such a long lifetime is the same in this picture as we have explained in the model of rotations around a symmetry axis: Two nucleons with aligned spins gain energy because their residual interaction is largest for wave functions with a large spacial overlap\* (see Sec. 4.4.8.). Therefore, these high spin levels are lower in energy than the neighboring states with smaller  $I$ -values, and fast  $\gamma$ -transitions are forbidden. In the description of

\* This effect has been called the MONA-effect (Maximal Overlap of the Nuclear wave function by Alignment [FPD 76]).

these nuclei by the mean field approach in a rotation about a symmetry axis, the same effect shows up in the fact that (as discussed in Fig. 3.18) aligned levels with maximal  $\alpha$ -values and oblate density distribution are shifted downwards in energy because of their large overlap with the oblate core.

Both methods—shell model calculations in a spherical basis based on angular momentum coupling techniques and cranking calculations in a slightly deformed well—are certainly hard to compare. The spherical shell model is certainly much better (though it takes more effort) as long as one can assume the spherical core to be inert, otherwise one has to take into account multiparticle-multipole configurations. It is therefore limited to the very close vicinity of magic nuclei. On the other side, the cranking model treats the residual interaction by a deformed well and is therefore much easier to handle over a wide range of nuclei. It allows, however, only very qualitative predictions, since it violates conservation of angular momentum and is microscopically derived only in the regions of well deformed nuclei with rotations perpendicular to the symmetry axis (see Sec. 11.4).